Instrumented undriven steering wheel to illustrate dynamic behavior of vehicles

A. Hajiahmad[1], A. Jafari[1*], A. Keyhani[1], H. Goli[2], B. No′dust[1]

(1. *Department of Agricultural Machinery Engineering, College of Agriculture and Natural Resources, University of Tehran, Karaj, Iran*;

2. *Department of Agricultural Machinery Engineering,   Science and Research Branch, Islamic Azad University, Tehran, Iran*)

Abstract: In this paper, a low-cost dynamometer for undriven, steered wheels is described.   The dynamometer was produced to determine whether such an instrumented mechanism is practical.   Four S-beam load cells and two opto-counters were used to obtain all moments, forces, and points of their application.   Overturning, aligning, and rolling resistance moments besides vertical force are directly measured by the load cells.   The opto-counters detect wheel angular velocity and steering angle. The dynamometer evaluation results showed significant correlation between expected values and measured data with high accuracy.   Wheel dynamic behavior can be defined according to dynamic and kinematic analysis in which relative calculations have minimum simplifying assumptions.

1   Introduction

Tires are the supporter part of vehicles against ground. All forces acting on a vehicle are transferred to the ground through tires.   The simulation of wheeled vehicles' performance and dynamic behavior requires determination of the forces acting on the tires (Karafiath, 1986).   Therefore, having information about components of these forces along three perpendicular axes is inevitable for dynamic analysis of a vehicle.   One of the commonly used axis systems recommended by the Society of Automotive Engineers (SAE) is shown in Figure 1.   According to the SAE (1976), origin of this system and center of the contact region of tire-ground are coincided.

*O*verturning and *rolling resistance* moments are applied to the tire, due to vertical force.   Because it is not exerted on center of the contact patch, and tangential forces have a lever arm.   Clearly, these moments are

influenced by angles of camber and castor.
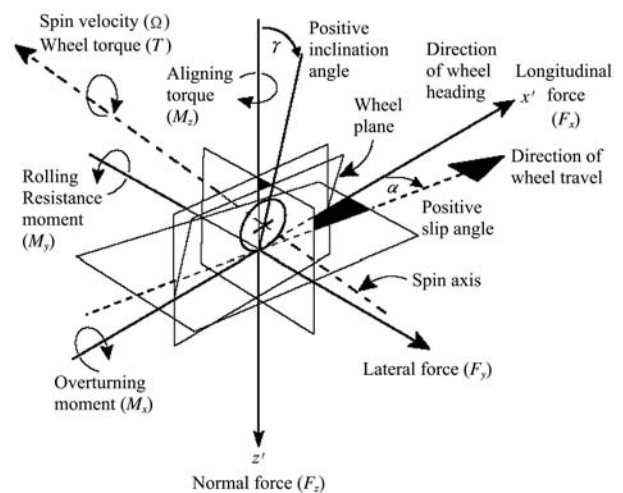
Figure 1   SAE tire coordinate axes and terminology (SAE, 1976)

The vertical (normal) force acting on a tire is induced by the chassis and vertical component of pulling force, interesting to vehicle designers for tire selection and assessing the suspension and cushioning behavior. Increase in vertical force leads a better tire-ground contact and decreases tire slippage which causes improvement in vehicle steerability.   On the other hand,

this component of the tire-ground force affects soil parameters and becomes more important when the soil is used for crop yielding. Soil compaction is produced from normal forces when the bearing capacity is reached (Liu et. al. 2009).

Longitudinal force is mainly generated by rolling resistance, drawbar pull and inertia force, while the lateral force is caused by cornering behavior, asymmetric drawbar pull and motion on slopes (Reimpell et. al. 2001; Wong, 2001). Steered wheels are more exposed to lateral force, because of their angle to the longitudinal axis of vehicle when cornering. Soil lateral and longitudinal forces displace soil and form ruts. Also, longitudinal forces produce wheel slip. Turning vehicles add a lateral force to the soil, displacing the soil out of the wheel track and towards the outside of the turn. Ruts can decrease plant development by damaging the root system (Althoff and Thien, 2005; Ayers,1994) .

When tangential (longitudinal and lateral) forces do not exert on the center of contact patch, these forces will induce a moment about z axis. This moment is known as *aligning torque* or *bore moment* which resists attempted turn and is the source of *understeer* effect (Gillespi, 1992; Wong, 2001). Direction control is implemented by applying a torque to the steering wheel that is then transmitted through a mechanical system to the steering tires, which are usually the front wheels. The required sensitivity is provided by the torque the steering system exerts on the driver through the aligning *torque* and the contact forces at the tire-ground interface. These, in turn, depend upon the geometry of the steering system (caster angle, toe in, offsets, etc.) (Reimpell et. al., 2001).

A lot of research has been conducted about measurement of contact forces and moments in dynamic mode. Most of which are related to theoretical analysis (Grečenko, 2007) either by mathematical modeling, that is based on the representation of a wheel as a mechanical system (Ivanov et. al., 2010) or with application of numerical methods(Hambleton and Drescher, 2009; Shoop, 2001; Tönük and ünlüsoy, 2001). Also, empirical measurement approach can be found in few papers. These experiments usually are conducted in soil bins(Karafiath, 1986; Gee-clough and Sommer, 1981; Gotteland and benoit, 2006; Kawase et. al., 2006; Krick, 1973; Raheman and Singh, 2004) , and rarely perform in real conditions by field tests (Besselink, 2004; Li and Sandu, 2007; Oida, 1983; Pearson and Bevly, 2007).

Krick (1973) and Raheman and Singh (2004) measured the drive- and side- force behavior of driven wheels running with side slip in a soil bin. Also measurement of the steering forces at low speed and zero camber angles were carried out on undriven, angled wheels in a soil bin by Gee-Clough and Sommer (1981).

In order to define turning behavior of an articulated tractor,Oida (1983) measured tire lateral force by attaching four strain gauges on its driving axle housing. Besselink (2004) developed a vehicle to study the tractive performance and designed a dynamometer consisting of an S-type load cell to measure dynamic force in longitudinal axis. To verify their suggested model, Pearson and Bevly (2007), measured lateral force of a tire using a dynamometer. Itoh (1994) presented his measuring method of vertical, longitudinal and lateral forces, which act on tires of a four-wheel drive and four-wheel steering agricultural tractor. He also measured longitudinal and lateral slip of the tires. Baffet et al. (2009) applied a very expensive dynamometric hub for measuring forces and moments acting on tires of an on-road vehicle to study the dynamic behavior of wheel-road interface. However, one can find some methods of measuring tire forces and moments in the literature, but they are limited to measure only one or two parameters or they have no ability to be installed on a real vehicle or the method is not economical. Therefore, this paper presents a low cost flexible method for measuring forces and moments in addition to application points of forces acting on undriven steering wheels, which are able to rotate about y and z axis.

2 Dynamometer explanation

In order to measure contact forces and moments, each steering wheel of a prototype vehicle, is equipped with four S-beam load cells. Since S-beam load cells are only able to measure tensile and compressive forces along their axes, it is necessary to omit the effect of other unwanted

forces and moments.   These load cells were used for measuring tire normal load (F_z), overturning moment (M_x), rolling resistance moment (M_y) and aligning *torque* (M_z).

2.1   Vertical force (F_z)

S-beam load cells are relatively easier to set up when they are in tension mode than compression (Bagad, 2008). Therefore, in spite of being compressive in nature, the normal load was measured in a way that the weight of vehicle induced a tension force on the load cell as shown in Figure 2.   Having caster angle and tangential forces in steering wheels, moments about x and y axes are generated, which are absorbed through frictionless, low clearance bushings for reading the vertical force accurately by the load cell 1.

a. 3D view

d. Top view of the contact patch

b. Side view

c. Front view

Figure 2   Schematic view of the dynamic measurement system:

Since this load cell is not able to measure weight of the parts standing below (W_f), its value is manually added to the dynamic weight read by load cell 1.

2.2   Overturning and rolling resistance moments (M_x and M_y)

Moment transducers are more expensive than S-beam force ones.   Therefore, overturning and rolling resistance moments were measured implicitly through forces taken by S-beam load cells multiplied by the normal distance of forces from the center of moments. M_x and M_y measurement system were designed in a way that center of moments were coincided.   To satisfy this purpose, a universal joint were used to transfer aligning *torque* from steering system to wheel and also provide two degrees of freedom in x and y axes.   Figure 2 displays the M_x and M_y measurement mechanism by means of load cells 2 and 3, assisted by Equations (1) and (2).

$$M_x = F_2 \cdot z_L \qquad (1)$$

$$M_y = F_3 \cdot z_L \qquad (2)$$

2.3   Aligning torque (M_z)

Aligning *torque* (bore moment) was calculated through multiplying turning force by its normal distance from center of moment, or:

$$M_z = F_{st} \cdot L_{st} \qquad (3)$$

where, F_{st} is the steering wheel turning force and can be determined through a simple analysis from the force

measured by load cell 4 according to Figure 3. It was ideal to install load cell 4 on the draglink as it is a two-force member without shear force, disturbing the force read by S-beam load cells. Not only shear force exerted on the load cell was negligible because of the small angle of β, but also the load cell installation on the cylinder shaft was easier.
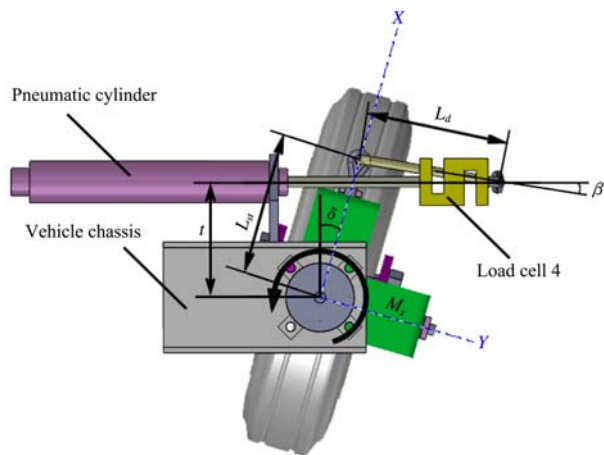
Figure 3   Top view of steering system

Steering system actuator is a pneumatic cylinder in the experimental vehicle. Drag link is converting the reciprocating motion of cylinder shaft to angular motion of steering arm. Decomposing the drag link internal force into two components in directions of perpendicular and along steering arm, F_{st} value can be obtained from Equation (4).

$$F_{st} = F_4 \cos \beta \cos(\delta - \beta) \qquad (4)$$

where, δ is steering angle measured by means of an opto-counter with a precision of half a degree; and β is calculated through Equation (5).

$$\beta = \sin^{-1}\left(\frac{L_{st} \cos \delta - t}{L_d} \right) \qquad (5)$$

2.4 Longitudinal force (F_x) and longitudinal distance between vertical force and center of contact patch (x_z)

Knowing rolling resistance moment (M_y), vertical force (F_z) and vertical distance between longitudinal force and center of universal joint (z_x), calculation of F_x and x_z becomes possible. In this calculation, accurate length of R_r depends on point of rolling resistance force application. According to Figure 2b changes in vertical position of this point is negligible in contrast with rolling radius, so in corresponding equations R_r is substituted with

measured distance between wheel center and ground surface. Since the friction of pivoting center of the tire is negligible, its value has been ignored and the wheel center acts as a pin joint. Therefore, it cannot exert any moment and tire longitudinal and vertical forces can be transmitted to this point ($F_x = F'_x$ and $F_z = F'_z$). Taking moments about point O, Equation (6) is obtained,

$$M_y = F'_z \cdot x_c - F'_x(z_x - R_r) \qquad (6)$$

With which F'_x is simply calculated considering Equation (2). Also, when moments about wheel center are taken, Equation (7) is derived to obtain x_z.

$$F_z \cdot x_z = F_x \cdot R_r \qquad (7)$$

2.5 Lateral force (F_y) and lateral distance between vertical force and center of contact patch (y_z)

Lateral force and the distance y_z are obtained when are known, according to Figure 2c. Taking moments about point O, Equation (8) is obtained.

$$M_x = F_y \cdot z_y + F_z \cdot y_z \qquad (8)$$

In other way:

$$M_x = F_{yz} \cdot r_{yz} \qquad (9)$$

Magnitude and direction of vector F_{yz} is defined with F_{yz} and θ_{yz} where they are calculated from Equations (10) and (11).

$$F_{yz} = \sqrt{F_y^2 + F_z^2} \qquad (10)$$

$$\theta_{yz} = \tan^{-1}\left(\frac{F_y}{F_z} \right) \qquad (11)$$

Moving resultant force of F_y and F_z along F_{yz}, M_x can be rewritten similar to Equation (12).

$$M_x = F_y \cdot r_{yz} \sin \theta_{yz} + F_z \cdot r_{yz} \cos \theta_{yz} \qquad (12)$$

Geometric analysis of forces generates Equation (13) as follows:

$$r_{yz} = y_z \cos \theta_{yz} + z_y \sin \theta_{yz} \qquad (13)$$

Equations (8), (9), (10), (12), and (13) form a system of equations with five unknown variables (r_{yz}, θ_{yz}, F_y, F_{yz}, and y_z) which is simply solvable.

2.6 Normal distances between tangential forces and center of contact patch (x_y and y_x)

Distances between tangential forces and center of contact patch (Pneumatic trails) can be found according to Figure 2d, through solving the system of equations given in Equations (14)-(17), in which F_x and F_y values are

recalled from parts 2.4 and 2.5.

$$M_z = F_x \cdot y_x + F_y \cdot (x_c + x_y) \qquad (14)$$

$$M_z = F_{xy} \cdot r_{xy} \qquad (15)$$

$$M_z = F_x \cdot r_{xy} \sin\theta_{xy} + F_y \cdot r_{xy} \cos\theta_{xy} \qquad (16)$$

$$r_{xy} = y_x \cos\theta_{xy} - x_y \sin\theta_{xy} \qquad (17)$$

3   Dynamometer development

Determining forces and moments acting on the steering tires of developed vehicle requires solution of above equations.   These equations have known parameters which their values follow the vehicle and its steering system specifications.

Each load cell has an output voltage.   These voltages in addition to output pulses from two opto-counters detecting steering angle and wheel angular velocity are transmitted to an Electronic Process Unit (EPU).   The EPU continuously records receiving data.   When the experiments were done, the EPU should be connected to a PC to transfer data for off-line analysis.

3.1   Load cell 1 capacity determination

The load cell 1 displays the dynamic weight acting on steering wheel from vehicle chassis.   The weight acting on each steering wheel on a flat surface in static mode is:

$$W_s = \frac{i \cdot W}{2} \qquad (18)$$

Traversing along steeps, moving on uneven surfaces, and sharp braking will increase wheel dynamic vertical load; which needs load cells with higher capacity, preventing from damage.   On the other hand, as the capacity of the load cell increases the data resolution and measurement precision will decrease, so a tradeoff between load cell safety and output resolution should be considered.   Therefore a safety factor of 2 seems to be appropriate for the selection of the load cell 1, resulting in the Equation (19) for detecting the maximum value of F_1.

$$F_{1max} = W_{dmax} = 2 \cdot W_s \qquad (19)$$

3.2   Load cell 2 capacity determination

The load cell 2 measures the moment of lateral and vertical forces about tire longitudinal axis.   The main part of this moment is due to tire lateral force, and vertical force effect is negligible because of its small lever arm (see Figure 2c).   According to Gee-Clough

and Sommer [15], maximum lateral force coefficient (C_{sfmax}) for a tire 4.00-8 is 0.85, occurring at maximum slip angle of 30° on a soil surface with a mobility number () of 9, where:

$$\mu = \frac{CI \cdot b \cdot d}{F_z} \sqrt{\frac{\Delta}{h}} \cdot \frac{1}{1 + b/2d} \qquad (20)$$

Since the tire selected for the steering wheel of the prototype vehicle is the same as mentioned tire, the maximum lateral force was determined by maximum dynamic weight assisted by Equation (21):

$$F_{ymax} = C_{sf\,max} \cdot W_{d\,max} \qquad (21)$$

This force generates a moment about center of universal joint with lever arm of z_y exerting a force to the load cell 2 calculated by Equation (22) .

$$F_{2max} = \frac{z_y \cdot F_{ymax}}{z_L} \qquad (22)$$

3.3   Load cell 3 capacity determination

The load cell 3 measures the moment caused by longitudinal and vertical forces about Y axis.   According to Equation (7) maximum longitudinal force occurs when pneumatic trail and vertical force are at the highest value, while rolling radius is minimal, such condition occurs when the tire is according to Figure 4 moving across a rigid step. Substitution of M_y from Equation (2) in Equation (6) results in Equation (23).

$$F_{3max} = \frac{F_{1max} \cdot [x_c R_r - x_z(z_x - R_r)]}{R_r \cdot z_L} \qquad (23)$$
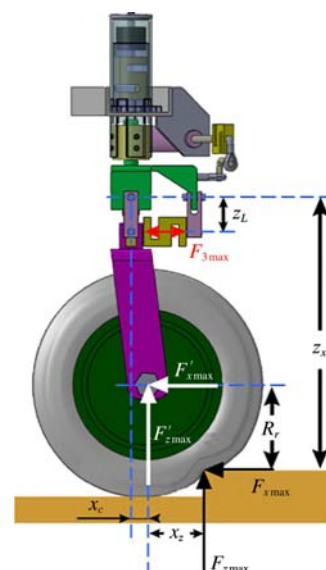
Figure 4   Condition in which the rolling resistance moment is at highest level

3.4　Load cell 4capacity determination

The load cell 4 measures the moment generated by tangential forces about z axis. Attending to maximum longitudinal and lateral forces obtained above, maximum resultant force ($F_{xy\ max}$) will be derived from Equation (10). Assuming a maximum lever arm of r_{xymax}, maximum force value of load cell 4 in different steering angles will be calculated using Equations (3), (4), (5), and (15) as below:

$$F_{4\max} = \frac{F_{xy\max} \cdot r_{xy\max}}{L_{st} \cos\beta \cos(\delta - \beta)} \qquad (24)$$

4　Dynamometer verification

4.1　Normal load (F_z)

To verify precision of normal load measurement, the wheel placed on a scale. Data determined by the load cell should be equal to subtraction of the weight of parts standing under load cell1 (W_f) from the value showed by the scale (W_s); so before assembly of the wheel, this weight had been measured. According to Figure 5a, the added loads on the wheel should satisfy the following relation.

$$W_s - W_f = F_1 \qquad (25)$$

In the Equation (25) as the coefficient of determination is higher, the load cell 1 has better performance.

4.2　Overturning moment (M_x)

To evaluate performance of the load cell 2, the steering wheel lifted, so that the reaction forces from the ground don't exert on it. Then, side force exerted on the wheel center with a handhold and connected load cell as shown in Figure 5b. Taking moment about the universal joint center the Equation (26) is derived:

$$F_2 = \hat{F}_y (z_y - R_r) / z_L \qquad (26)$$

Comparing the calculated values from Equation (26) ($\hat{F}_2$) and measured data (F_2), the dynamometer performance in determination of M_x will be specified.

4.3　Rolling resistance moment (M_y)

To validate the data recorded by the load cell 3 and to ensure accuracy of equations, a yoke connected to the wheel center parallel to the ground surface as is shown in Figure 5c. Pulling handhold along the wheel longitudinal

axis, the calibrated load cell measures the $\hat{F}_x$ while normal load was shown by load cell 1. These two forces generate a moment about Y axis related to the recorded values of the load cell 3 through Equations (2), (6), and (7). While verification was doing, the wheel was stood on a rigid surface and the tire pressure was at maximum level, therefore the rolling resistance was negligible. In other word, the F_z was along the wheel center or in Equation (7), x_z is equal to zero. It means F'_x can be substituted by $\hat{F}_x$ in Equation (6). Comparing the calculated values of $\hat{F}_3$ in Equation (2) and its measured value (F_3), the M_y data accuracy is accessible.

a. Normal load　　　　b. Rolling resistance moment

c. Overturning moment　　　　d. Aligning torque
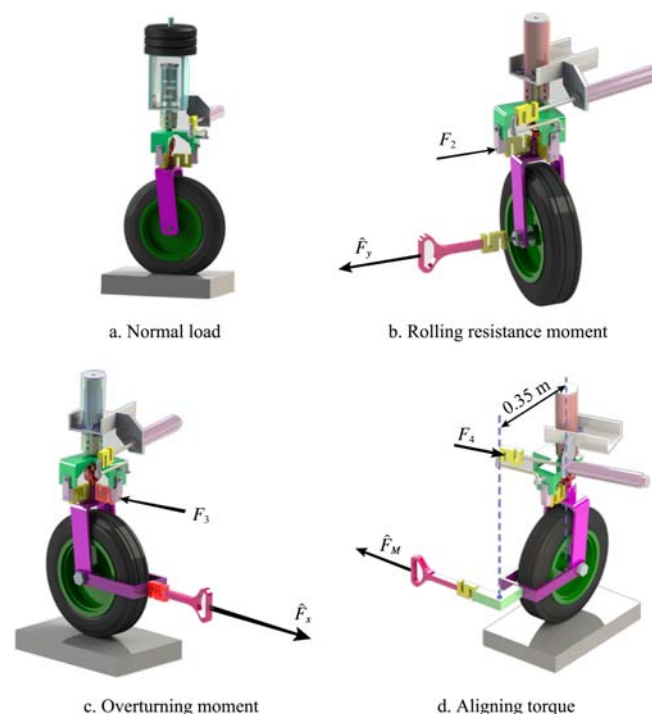
Figure 5　Verification method of each load cell of the dynamometer

4.4　Aligning torque (M_z)

According to Figure 5d a lateral force parallel to the ground surface assisted by a handhold was acted on a point with a distance of 35 cm from wheel pivoting axis (king pin). Equations (3)-(5) show the relations for calculating the value of load cell 4 ($\hat{F}_4$).Comparing with the recorded values of the load cell 4 (F_4) helps to obtain the accuracy of aligning torque measurement.

5　Results and discussion

The instrumented undriven steering wheel was

developed and installed in a prototype tractor as is shown in Figure 6.   The used tire was a 4.00-8, 6-bias ply having a castor angle of 5 degree.   Other specifications of the vehicle are denoted in Table 1 with which their values are constant.

a. Total view   b. Close view showing steering
                          angle transducer apparently
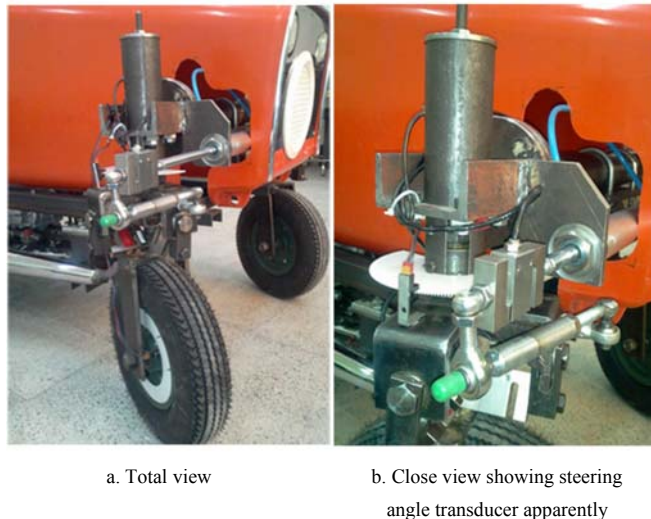
Figure 6   Experimental steering wheel (with a 4.00-8, 6 ply tire) equipped with measuring tools

Table 1   Vehicle and steering system specifications

Parameter	Value	Parameter	value
φ	0 deg.	L_{st}	0.172 m
γ	5 deg.	L_d	0.190 m
x_c	0.033 m	t	0.125 m
z_L	0.052 m	W	3675 N
$z_x - R_r$	0.296 m	W_f	281 N
$z_y - R_r$	0.296 m	i	0.4
d^*	0.398 m	h	0.083 m
R_r	0.195 m		

Note: * When the wheel load is picked up and tire pressure is 200 kPa.

5.1   Determination of the load cells capacity

According to the Table 1 and Equations (18)-(22), two load cellswithcapacityof 150 and 1,200 kgf selected for the load cells 1 and 2 respectively, which were well responding in different situations.   In order to detect the capacity of the load cell 3, a 5 cm height step was considered as mentioned in part 3.3, and corresponding values of R_r and x_z were measured, which were equal to 153 mm and 108 mm respectively.   Substituting these values in Equation (23) resulted in 4,970 N for maximum force of F_3.   Therefore, a load cell with a capacity of 500 kgf was selected satisfying various conditions.   The load cell 4 capacity was selected considering Equation

(24) in which $r_{xy\ max}$ was assumed to be 5cm and $F_{xy\ max}$ was calculated by Equation (10).   Since β is a function of the steering angle (δ), and δ varies between ±40°, the F_4 is in maximum value when δ is -40 degree, in which it is about 557 N.   Therefore, a load cell with a capacity of 60 kgf was applied measuring aligning torque.

5.2   Dynamometer verification results

Figure 7 ashows the recorded data by the load cell 1 versus the scale values verifying normal load.   The offset indicates the weight of the parts standing under the load cell 1(W_f) which is immeasurable by load cell 1.   Before the assembly of the wheel, weight of this section had been measured by the scale and was equal to 281 N which its difference with the offset of the regression line (286.45) is insignificant.

In Figure 7b the data recorded by the load cell 2 is depicted versus calculated values from Equations (1) and (8).   This graph has also differences from 45 degree line due to directional deviation of handhold from lateral axis and load cell2 axis.   In spite of that, having a high coefficient of determination indicates high performance of the dynamometer in overturning moment measurement.

Figures 7c and 7d illustrate the recorded data by the load cell 3 versus expected values from Equations (2) and (6) ignoring rolling resistance as is described in part 4.3.   These figures show the values in two cases: 1- when the wheel was stood on a rigid surface (Figure 7c), and 2- when it was lifted ($F_z = 0$) (Figure 7d).   As was depicted, the recorded data by the load cell 3, when the wheel was lifted, had less offset with 45 degree line.   The offset is due to ignoring displacement of the application point of ground reaction force from the wheel center.   In the whole working range of load cell 3, minor differences are visible from 45 degree line.   These differences are because of directional deviation of handhold from tire longitudinal axis and load cell axis, which appear more, when the tire is lifted.

Figure 7e shows variation of F_4 values versus different steering angles which is determined by Equations (3), (4), (5), and (14) in different forces of $\hat{F}_M$.   Smooth curves are extracted from equations and the points indicate measured values.   Coefficients of

determination are high enough to ensure measurement precision of the dynamometer.

a. Normal load

b. Overturning moment

c. Rolling resistance moment (F_z=800 N)

d. Rolling resistance moment (F_z=0 N)

e. Aligning torque
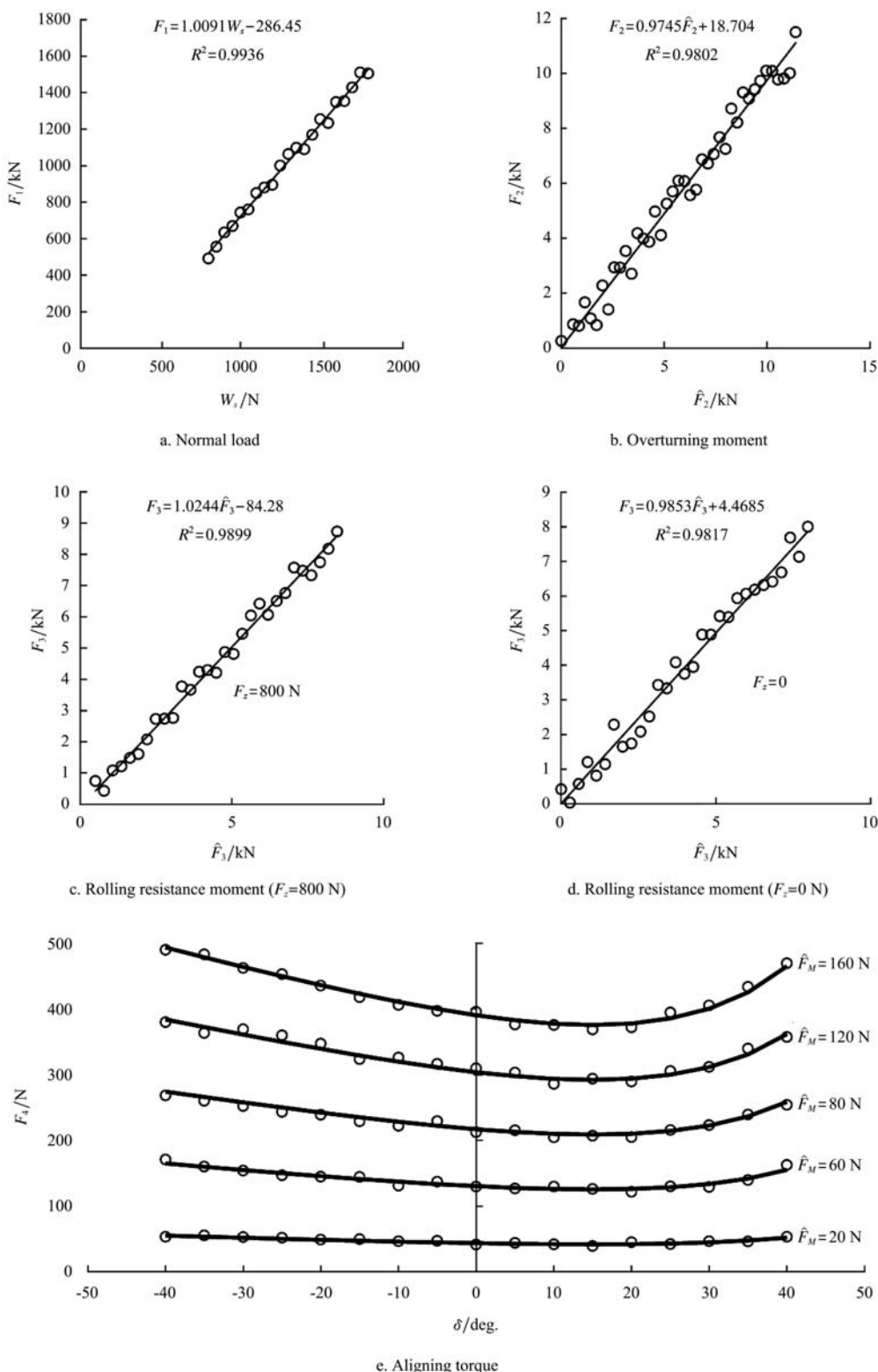
Figure 7   Graphs of the dynamometer verification

6   Conclusion

The mechanism outlined in this paper demonstrates the feasibility of measuring all forces and moments acting on an undriven steered wheel. In this mechanism the low cost common S-beam load cells have been used which in contrast to manual strain gauges installation on structure has greater accuracy; however, it needs more development. The cost of the S-beam load cells is lower than that of dynamometric hubs and torque transducers,

while their precision is sufficient.

In this paper because of having no knowledge about application point of rolling resistance, tire longitudinal force has an expected error.   If another mechanism was developed to measure longitudinal force, the accurate position of this force application would be obtained.

Acknowledgment:

Nomenclature

b	Tire width [m]
C_{sf}	Lateral (side) force coefficient of tire [-]
CI	Soil cone index [Pa]
d	Tire diameter [m]
$\hat{F}_M$	Calibrated force tending to turn steering wheel [N]
F_{st}	The force, normal to steering lever [N]
F_x	Longitudinal force acting on tire [N]
F'_x	Longitudinal force acting on wheel center [N]
$\hat{F}_x$	Calibrated longitudinal force exerting on the wheel center [N]
F_{xy}	Resultant force of F_x and F_y [N]
F_y	Lateral force acting on tire [N]
$\hat{F}_y$	Calibrated lateral force exerting on the wheel center [N]
F_{yz}	Resultant force of F_y and F_z [N]
F_z	Vertical force acting on tire [N]
F'_z	Vertical force acting on wheel center [N]
F_1	The force shown by load cell 1 [N]
F_2	The force shown by load cell 2 [N]
$\hat{F}_2$	The predicted force for load cell 2 [N]
F_3	The force shown by load cell 3 [N]
$\hat{F}_3$	The predicted force for load cell 3 [N]
F_4	The force shown by load cell 4 [N]

g	Gravitational acceleration [9.8 Nkg^{-1}]
h	Tire section height [m]
i	The ratio of forward axle weight to the vehicle weight [-]
L_d	Drag link length [m]
L_{st}	Steering arm [m]
M_x	Overturning moment [N.m]
M_y	Rolling resistance moment [N.m]
M_z	(Self) aligning torque[N.m]
r_{xy}	Lever arm of F_{xy} [m]
r_{yz}	Lever arm of F_{yz} [m]
R_r	Tire rolling radius [m]
t	Normal distance between cylinder shaft and kingpin [m]
W	Prototype vehicle weight [N]
W_d	Dynamic weight on steering tire [N]
W_f	Weight of the parts standing below the load cell 1 [N]
W_s	The static weight on steering tire [N]
x_c	Longitudinal distance between kingpin and center of contact patch [m]
x_y	Longitudinal distance between center of contact patch and F_y [m]
x_z	Longitudinal distance between center of contact patch and F_z [m]
y_x	Lateral distance between center of contact patch and F_x [m]
y_z	Lateral distance between center of contact patch and F_z [m]
z_L	Vertical distance between center of universal joint and load cell axis [m]
z_x	Vertical distance between center of universal joint and F_x [m]
z_y	Vertical distance between center of universal joint and F_y [m]
α	Slip angle of tire [deg.]
β	The angle between cylinder shaft and drag link [deg.]
γ	Camber angle of tire [deg.]
δ	Steering angle [deg.]
Δ	Tire deflection under load [m]
θ_{xy}	The angle between F_{xy} and longitudinal axis [deg.]
θ_{yz}	The angle between F_{yz} and vertical axis [deg.]
μ	Mobility number [-]
φ	Castor angle of tire [deg.]

References

Althoff, P. S., and S. J. Thien. 2005. Impact of M1A1 main battle tank disturbance on soil quality, invertebrates and vegetation characteristics. *Journal of Terramechanics*, 42(3): 159-176.

Ayers P. D.   1994. Environmental damage from tracked vehicle operation. *Journal of Terramechanics*, 31(3): 173-183.

Baffet, G., A. Charara, and D. Lechner. 2009. Estimation of vehicle side slip, tire force and wheel cornering stiffness. *Journal of science*, 17(11): 1255-1264.

Bagad, V. S. 2008. *Mechatronics*, 4th ed. Technical Publications Pune, Pune.

Besselink, B. C. 2004. Development of a vehicle to study the tractive performance of integrated steering drive systems. *Journal of Terramechanics*, 41(4): 187-198.

Gee-clough, D., and M. S. Sommer. 1981. Steering forces on undriven angled wheels. *Journal of Terramechanics*, 18(1): 25-49.

Gillespi, T. D. 1992. *Fundamentals of Vehicle Dynamics*. Society of Automotive Engineers, Inc.,Warrendale, PA.

Gotteland, P. H., and O. Benoit. 2006. Sinkage tests for mobility study, modeling and experimental validation. *Journal of Terramechanics,* 43(4):451-467.

Grečenko, A. 2007. Thrust and slip of truck determined by the compression-sliding approach. *Journal of Terramechanics*, 44(6): 451-459.

Hambleton, J. P., and A. Drescher. 2009. Modeling wheel-induced rutting in soils: rolling. *Journal of Terramechanics,* 46(2): 35-47.

Itoh, H., A. Oida, and M. Yamazaki. 1994. Measurement of forces acting on 4WD-4WS tractor tires during steady-state circular turning on a paved road. *Journal of Terramechanics*, 31(5): 285-312.

Ivanov, V., B. Shyrokau, K. Augsburg, and V. Algin. 2010. Fuzzy evaluation of tyre-surface interaction parameters. *Journal of Terramechanics*, 47(2): 113-130.

Jazar, R. N. 2008. *Vehicle Dynamics: Theory and Application*. Springer Science, New York.

Karafiath, L. 1986. Tire-soil interaction model for turning (steered) tires. *Journal of Terramechanics*, 23(3): 153-169.

Kawase, Y., H. Nakashima, and A. Oida. 2006. An indoor traction measurement system for agricultural tires. *Journal of Terramechanics*, 43(3): 317-327.

Krick, G. 1973. Behavior of tyres driven in soft ground with side slip. *Journal of Terramechanics*, 9(4): 9-30.

Li, L., and C. Sandu. 2007. On the impact of cargo weight, vehicle parameters, and terrain characteristics on the prediction of traction for off-road vehicles. *Journal of Terramechanics*, 44(3): 221-238.

Liu, K., P. Ayers, H. Howard, and A. Anderson. 2009. Influence of turning radius on wheeled military vehicle induced rut formation. *Journal ofTerramechanics*, 46(2): 49-55.

Oida,A. 1983. Turning behavior of articulated frame steering tractor –I. Motion of tractor without traction. *Journal of Terramechanics*, 20(3/4): 153-165.

Pearson, P.,and D. M. Bevly. 2007. Modeling and validation of hitch loading effects on tractor yaw dynamics. *Journal of Terramechanics*, 44(6): 439-450.

Raheman, H., and R. Singh. 2004. Steering forces on undriven tractor wheel. *Journal of Terramechanics*, 40(3): 161-178.

Reimpell, J., H. Stoll, and J. W. Betzler. 2001. *The Automotive Chassis: Engineering Principles*, 2[nd]ed. Butterworth-Heinemann, Oxford, 2001.

Shoop, A. S. 2001. Finite element modeling of tire terrain interaction, Engineer Research & Development Center/Cold Regions Research and Engineering Laboratory, Technical Report-01-16, Vicksburg, Miss.: U. S. Army crop of engineers.

Tönük, E., and Y. S. ünlüsoy. 2001. Prediction of automobile tire cornering force characteristics by finite element modeling and analysis. *Journal of Computer and Structures*, 79(13): 1219-1232.

Vehicle Dynamics Terminology, SAE J670e, Society of Automotive Engineers, Inc.,Warrendale, PA, July 1976.

Wong, J. Y. 2001. *Theory of Ground Vehicles*,3rd ed. John Wiley and Sons, New York.